Nanoscale

Accepted Manuscript

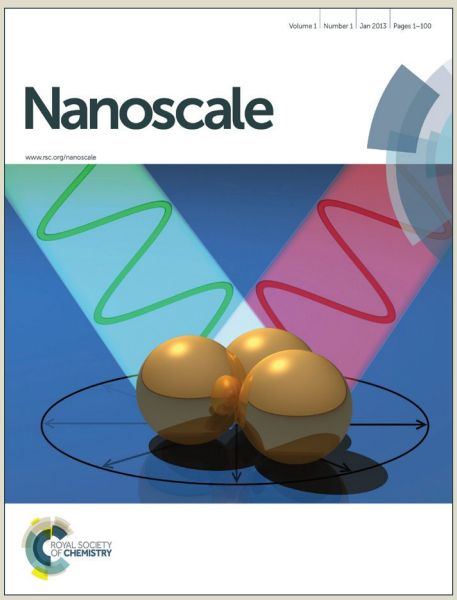

ROYAL SOCIETY OF CHEMISTRY

www.rsc.org/nanoscale

Amphiphilic Fullerenes/ZnO Hybrids as Cathode Buffer Layer to Improve Charge Selectivity of Inverted Polymer Solar Cells

Ting Hu[a], Lie Chen[a,b], Kai Yuan[a], Yiwang Chen*[a,b]

[a]College of Chemistry/Institute of Polymers, Nanchang University, 999 Xuefu Avenue, Nanchang 330031, China

[b]Jiangxi Provincial Key Laboratory of New Energy Chemistry, Nanchang University, 999 Xuefu Avenue, Nanchang 330031, China

*Corresponding author. Tel.: +86 791 83968703; fax: +86 791 83969561. E-mail: ywchen@ncu.edu.cn (Y. Chen).

Abstract

Two types of novel fullerene derivative/ZnO hybrids were prepared by physical blending amphiphilic fullerene-end-capped poly(ethylene glycol) (C60-PEG) with ZnO nanocrystals (ZnO/C60-PEG) and by *in situ* growth ZnO from C60-PEG (ZnO@C60-PEG) at relatively low temperature. The C60-PEG could act as n-doping on the ZnO while the PEG side chain of C60-PEG could passivate the defects of the ZnO at the same time, consequently increased the lowest unoccupied molecular orbital (LUMO) level. Compared with the ZnO/C60-PEG by physical blend approach, the ZnO@C60-PEG by growth approach showed more favorable morphology and higher electron mobility by developing a homogenous network. In consequence, the efficiency of the inverted polymer solar cells based on thieno[3,4-b]-thiophene/benzodithiophene (PTB7):[6,6]-phenyl C_{71}-butyric acid methyl ester ($PC_{71}BM$) is raised to 8.0% for ZnO@C60-PEG cathode buffer layer and to 7.5% for ZnO/C60-PEG cathode buffer layer with improved long-term stability.

Keywords: Charge selectivity; Zinc oxides; Fullerenes; Hybrids; Nanocrystals

1. Introduction

Due to the superior advantages of mechanical flexibility, lightweight, semi-transparent characteristics, solution-based processing, and large area roll-to-roll manufacturing at low temperatures, polymer solar cells (PSCs) has become the hottest research topic over the past decades.[1-3] In the traditional PSCs, the conjugated polymers and fullerenes blends as photoactive layer for efficient excitons dissociation in the interpenetrating networks has been extensively studied, but the performance is comparatively low. Hence, various methods applied to improve the performance of PSCs, such as designing new active materials,[4-7] developing more efficient device processing,[3, 8, 9] and using effective and stable device structure.[10, 11] A good interface plays a critical role in improving the performance of PSCs, so significant effort is also devoted on the interface engineering of PSCs. A wide range of materials have been explored as interfacial layers to optimize the PSCs, including conducting polymers,[12-14] metal oxides,[15-17] crosslinkable materials,[18, 19] conjugated polymer electrolytes,[20-22] self-assembled functional molecules[23-25] and graphene-based materials.[26-28] Metal oxides have received extensive attention owing to the high electron mobility, stable physical and chemical properties.

Among all the metal oxides, ZnO is environmentally friendly, relatively easy to be synthesized in large quantities and prepared at a low temperature. In addition, as an n-type semiconductor with a wide band gap, ZnO also has good optical transmittance, high electron mobility and excellent stability, which makes ZnO is a promising candidate as an efficient cathode buffer layer in PSCs.[29, 30] However, nanoparticles synthesized by sol–gel processes are full of defects, which can trap the carriers and decrease electron mobility. Besides, nanoparticles in solution tend to form agglomerates and precipitate, which also has a negative impact on the performance of the PSCs. Many approaches are developed to solve these problems. Amorphous TiOx was used to fill in the voids between ZnO nanoparticles and passivate the traps in the surface of ZnO.[31] Poly(ethylene glycol) (PEG)[32, 33] or poly(ethylene oxide) (PEO),[34] was also adopted to modified ZnO. It also reported using zinc acetate in 2-methoxyethanol as a precursor solution to prepare uniform sol-gel-derived ZnO

films at relatively low annealing temperature.[17] Nevertheless, the inorganic buffer layer has poor interfacial contact with the organic active layer, which results in bad electron extraction.[35] Thus, it is important to modify the interface to improve electron extraction in PSCs.

Herein, two types of novel fullerene derivative/ZnO hybrids were developed as cathode buffer layer to improve the performance of PSCs, which were prepared by physical blending amphiphilic fullerene-end-capped PEG (C60-PEG) with ZnO nanocrystal (ZnO/C60-PEG) and *in situ* growth ZnO from C60-PEG (ZnO@C60-PEG) at relatively low temperature. For two types of hybrids, the fullerene derivative not only acts as a modifier, but also produces an effect of n-doping. Meanwhile, the hydrophilic PEG side chain of C60-PEG could improve the dispersity of ZnO nanoparticles and passivate the defects on the surface of ZnO. In the ZnO@C60-PEG hybrids by growth approach, C60-PEG also can acts as a template for the *in situ* growth of ZnO nanocrystals to further form a uniform film with less defects and traps. Moreover, C60-PEG improves the compatibility of inorganic ZnO and organic active layer, enlarging the contact area between cathode buffer layer and active layer. And the lowest unoccupied molecular orbital (LUMO) level of ZnO is improved effectively by the n-doping of C60-PEG. Consequently, ZnO/C60-PEG by blend approach and ZnO@C60-PEG by growth approach substantially reduces the recombination of carriers, increases the electron mobility and enhances electron extraction, while ZnO@C60-PEG is more favorable. Meanwhile, the hybrid by *in situ* CdS growth from C60-PEG (CdS@C60-PEG) was prepared by the universal approach for improving charge selectivity. By applying fullerene derivative/ZnO hybrids as cathode buffer layer, the performance of the inverted PSCs reaches to 8.0% for ZnO@C60-PEG and 7.5% for ZnO/C60-PEG, respectively.

2. Results and Discussion

The chemical structures of the materials employed for the fabrication of device, and the inverted device architecture with the schematic diagram of two types fullerene

derivative/ZnO hybrids are presented in **Figure 1**. C60-PEG was synthesized by the Steglich esterification according to the literature[36] and the synthetic details are described in the experimental section. The chemical structure of C60-PEG was identified by ^{1}H NMR (**Figure S1**). ZnO@C60-PEG was obtained by *in situ* growth ZnO nanocrystals from C60-PEG and the ZnO@C60-PEG precursor solution was prepared following the process reported by Heeger *et al*[17] via adding C60-PEG with different weight. Here, ZnO@0.1%C60-PEG, ZnO@0.5%C60-PEG, ZnO@1%C60-PEG and ZnO@5%C60-PEG represent 0.1%C60-PEG, 0.5%C60-PEG, 1%C60-PEG and 5%C60-PEG in weight percentage was added in the ZnO precursor solution, respectively. However, the ZnO nanocrystals in the hybrid of ZnO/C60-PEG was synthesized according to the method reported by Beek *et al*.[37] ZnO/C60-PEG was prepared by physical blending the ZnO nanocrystals with C60-PEG. Similarly, we adopted the ZnO nanocrystals blending with 1%C60-PEG, 3%C60-PEG and 5%C60-PEG as ZnO/1%C60-PEG, ZnO/3%C60-PEG and ZnO/5%C60-PEG in weight percentage.

------**Figure 1**------

Atomic force microscope (AFM) was carried out to investigate the influence of C60-PEG on the dispersion of ZnO nanoparticles, and the AFM height images of ZnO prepared by Beek´s method and ZnO/C60-PEG by blend approach are exhibited in **Figure 2**. The pristine ZnO nanocrystals aggregate together to form large aggregates (**Figure 2a**) and present the roughest surface with root-mean-square (RMS) roughness value of 8.71 nm. When the C60-PEG was added, the large aggregates of ZnO were dispersed into nanoclusters with less domain boundaries. This is because the PEG side chain of C60-PEG could wrap the ZnO nanocrystals to avoid the aggregation, with the favor of the interaction between the ZnO and PEG[32]. All the modified samples process a relative smoother surface with a decreased RMS, which could improve the contact between the cathode buffer layer and the active layer.[30] The result is also consistent with TEM images of ZnO, ZnO/1%C60-PEG, ZnO/3%C60-PEG and

ZnO/5%C60-PEG (**Figure S2**). Compared with the pristine ZnO with a serious aggregation, the modified samples of ZnO blending with C60-PEG show a better dispersion.

In order to verify the effect of C60-PEG on the *in situ* growth of ZnO nanocrystals, transmission electron microscopy (TEM) measurement was employed to observe the morphology of ZnO prepared by Heeger's method and ZnO@1%C60-PEG by growth approach. As shown in **Figure 3a**, the pristine ZnO nanocrystals are sparse and scattered. In contrast, the ZnO@1%C60-PEG (**Figure 3b**) reveals the totally different morphology, showing a network structure with dense and homogenous ZnO nanocrystals. It should be noted that morphology of ZnO@C60-PEG is even more homogenous with well-dispersed ZnO nanocrystals than that of ZnO/C60-PEG by blend approach (**Figure S2**). Due to the interaction between the ZnO and PEG,[32] ZnO precursor can easily anchor on the PEG side chain, and the PEG side chain of C60-PEG could form a web-like tangle to provide a template for the *in situ* growth of ZnO nanocrystals. The energy dispersive X-ray (EDX) spectrum of ZnO@1%C60-PEG (inset in **Figure 3b**) has the same elements with the EDX spectrum of ZnO (inset in **Figure 3a**), which confirms the successful growth of ZnO. In addition, the corresponding high resolution transmission electron microscopy (HRTEM) images of ZnO (**Figure 3c**) and ZnO@1%C60-PEG (**Figure 3d**) are displayed. The lattice spacing of 0.26 nm is associated with (0002) lattice planes of ZnO.[38] Obviously, ZnO nanocrystals exist in the space of the network structure of C60-PEG to form a dense and uniform film. Besides, CdS growth *in situ* from C60-PEG (CdS@C60-PEG) was also adopted for the purpose of further demonstrating the universal approach. CdS nanocrystals were prepared by *in situ* growth with metal–xanthate precursor $[Cd(S_2COEt)_2(C_5H_4N)_2]$.[39] The pristine CdS nanocrystals are aggregated together to forming large aggregates (**Figure S3a**). When the C60-PEG was introduced, CdS@C60-PEG presents a network with CdS nanocrystals distributing uniformly (**Figure S3b**). By comparing the HRTEM image of pristine CdS (**Figure S3c**) with that of CdS@C60-PEG (**Figure S3d**), it is found that the CdS@C60-PEG has a better crystal with the presence of C60-PEG. Thus, we

can conclude that C60-PEG can acts as a universal template for *in situ* growth of nanocrystals.

------Figure 2------

------Figure 3------

X-ray photoelectron spectroscopy (XPS) was brought to research the composition of all the samples. **Figure 4a** shows the core level XPS spectra of Zn 2p of ZnO and ZnO@C60-PEG by growth approach. It could be observed that the binding energy of Zn 2p3/2 peak for pristine ZnO is located at 1021.2 eV, which is assigned to the Zn-O bonds.[40] Compared with the pristine ZnO, the binding energy of the Zn 2p3/2 peak for all the samples *in situ* growth in C60-PEG changes in different degrees. The Zn 2p3/2 peak shifts toward the higher binding energy by 0.1 eV for ZnO@0.1%C60-PEG, 0.2 eV for ZnO@0.5%C60-PEG and 0.2 eV for ZnO@1%C60-PEG. It implies that the electronic states of ZnO are different as literature reported,[41, 42] and C60-PEG exerts an effect of n-doping on the ZnO, similar to the Al-doped ZnO.[41] Nevertheless, the position of the Zn 2p3/2 peak for ZnO@5%C60-PEG shifts toward the lower binding energy by 0.1 eV with respect to the pristine ZnO, indicating that more intermolecular interaction between PEG side chain and ZnO exists in the ZnO@5%C60-PEG film and larger number of Zn atoms are bound to O atoms[43]. With the content of C60-PEG increasing, the interaction between PEG side chain and ZnO tends to be beyond the n-doping effect, resulting in the reverse shift of the Zn 2p3/2 peak. **Figure 4b** exhibits the core level XPS spectra of Zn 2p of ZnO and ZnO/C60-PEG by physical blend approach. The binding energy of Zn 2p3/2 peak for pristine ZnO is located at 1021.2 eV. When blend with C60-PEG, the position of the Zn 2p3/2 peak shifts toward the higher binding energy by 0.3 eV for ZnO/1%C60-PEG, by 0.2 eV for ZnO/3%C60-PEG and by 0.1 eV for ZnO/5%C60-PEG, respectively. The shift displacement decreases with the increase of the ratio of C60-PEG, which attributes to the stronger effect of the PEG side chain is beyond the n-doping effect of C60-PEG.

------Figure 4------

Since the surface of nanocrystals plays a critical role in the properties of the nanocrystals due to their high surface-to-volume ratio,[44, 45] the photoluminescence (PL) was applied to study the effect of C60-PEG on the surface defects of ZnO. The PL spectra under photoexcitation at 325 nm of ZnO and ZnO@C60-PEG by growth approach are represented in **Figure 5a**. The emission band at 371 nm is owing to the usual band-edge emission in the UV. However, the spectra for all the samples shows one broad emission in blue regions with two shoulders, one at 420 nm and the other at 440 nm. It is caused by the transitions involving Zn interstitial defect states as reported.[46] The intensity of the peak for pristine ZnO is much stronger than that for ZnO *in situ* growth in C60-PEG. It can be inferred that the C60-PEG passivates the shallow trap sites of ZnO because of the oxygen-rich PEG side chain,[34, 47] which can reduce the recombination of charge carriers. The passivation of defects and traps of ZnO can also be found in the ZnO/C60-PEG hybrids obtained by physical blend approach, as shown in **Figure 5b**.

------Figure 5------

Figure 6a shows Ultraviolet photo-electron spectroscopy (UPS) taken for two types of ZnO hybrids. The left panel is E_{cutoff} gained from the high binding energy cutoff of a spectrum,[48, 49] and the right panel provides E_{onset}^{HOMO}. The highest occupied molecular orbital (HOMO) level energies are calculated according to the equation.[49]

$$E_{HOMO} = h\upsilon - (E_{onset}^{HOMO} - E_{cutoff})$$

where hν is the incident photon energy of 21.2 eV. As a result, the HOMO energies for ZnO, ZnO@0.1%C60-PEG, ZnO@0.5%C60-PEG, ZnO@1%C60-PEG and ZnO@5%C60-PEG are -7.60 eV, -7.47 eV, -7.40 eV, -7.38 eV and -7.36 eV, respectively. By combining these HOMO energies with the optical band gap obtained from the UV–vis absorption spectra (**Figure 6b**),[50] the LUMO energy levels were

estimated as -4.29 eV for ZnO, -4.23 eV for ZnO@0.1%C60-PEG, -4.16 eV for ZnO@0.5%C60-PEG, -4.10 eV for ZnO@1%C60-PEG and -4.12 eV for ZnO@5%C60-PEG, which are summarized in **Table 1**. As shown in **Figure S4,** the LUMO energy levels of ZnO and ZnO/C60-PEG were estimated in the same way and the corresponding values are summarized in **Table S1**. The increased LUMO energy level of all the modified samples is ascribed to the n-doping of C60-PEG and the passivation of ZnO surface traps by C60-PEG. The decreased work function of the C60-PEG modified ZnO as cathode buffer layer could produce a better energy alignment in the device, thereby beneficial to the charge extraction and collection, and the enhancement of V_{oc} as well.[51]

------**Figure 6**------

-------**Table 1**-------

Since the C60-PEG can passivate the defects on the surface of ZnO nanocrystals, the electron mobility of ZnO nanocrystals is expected to be improved. Thus the space-charge-limited-current (SCLC) was employed by adopting electron-only devices (inset of **Figure 7a** and **Figure 7b**). The fitted curves using the SCLC model of two types of hybrids cathode buffer layer are presented in **Figure 7**, and the corresponding electron mobility calculated using the Mott–Gurney SCLC equation[52, 53] are listed in **Table S2** and **Table S3**. As the results shows, when physical blend with C60-PEG, the electron mobility of all ZnO/C60-PEG samples is higher than that of pristine ZnO, and the ZnO/3%C60-PEG presents the highest electron mobility of 8.11×10^{-4} cm^2 V^{-1} s^{-1}. Further improve the content of C60-PEG to 5%, the electron mobility of ZnO/5%C60-PEG drops, due to the increased loading of the insulated PEG side chain of C60-PEG. The X-ray diffraction (XRD) spectrum of the ZnO@3%C60-PEG (**Figure S5**) reveals the best crystallinity among these blend films. The same tendency of the electron mobility also can be observed in ZnO@C60-PEG systems by *in situ* growth approach. At the same time, when the loading of C60-PEG in the two type of films is the same, the sample with ZnO nanocrystals *in situ* growth

from C60-PEG delivers the higher electron mobility than that of blend one, e.g. The ZnO@1%C60-PEG presents the highest electron mobility of 9.75×10^{-4} cm^2 V^{-1} s^{-1}(**Table S2**), while ZnO/1%C60-PEG only shows 50% discount value. The priority of the *in situ* growth of ZnO from C60-PEG to the physical blend of the two components can be attributed to the more homogenous networks developed by *in situ* growth method.

------**Figure 7**------

The optical transmittance spectra of two types of hybrids are displayed in **Figure S6**. All of the films show similar spectra profiles with relative high optical transmittance, indicating they are all suitable for cathode buffer layers. The inverted device with the structure, ITO/ cathode buffer layer/ PTB7:$PC_{71}BM$/ MoO_3/ Ag, was fabricated by using two types of hybrids as cathode buffer layer. The current density−voltage (*J*-*V*) curves are shown in **Figure 8**, and the corresponding parameters of the devices are listed in **Table 2**. The detail preparation process of the devices is described in the experimental section. With better properties, the devices based on PTB7:$PC_{71}BM$ with ZnO@C60-PEG by growth approach as cathode buffer layer submit an improved PCE. Consequently, the device with ZnO@1%C60-PEG cathode buffer layer delivering the highest PCE of 8.0% with a short circuit current density (J_{sc}) of 15.86 mA cm^{-2}, an open circuit voltage (V_{oc}) of 0.733 V, a fill factor (FF) of 69.1%. The IPCE spectra in **Figure S7a** are well in accordance with the J_{sc} values. The enhancement of J_{sc} and FF could owe to the higher electron mobility of ZnO@C60-PEG cathode buffer layer. Besides, the amphiphilic property of C60-PEG should be taken into account, which helps to produce a good compatibility of inorganic cathode buffer layer and organic active layer. Meanwhile, the improved V_{oc} arises from the better energy alignment. The highest performance induced by the ZnO@1%C60-PEG is can be elucidated by its highest charge transport and the most restrained leakage current (**Figure S7b**), which implies that the recombination of charge decreases in the cathode buffer layer.[51, 54] In addition, compared with the bare ZnO, the performance of the inverted devices

by using ZnO/C60-PEG by blend approach also has been improved. The related *J-V* curves are displayed in **Figure 8b**, while the IPCE spectra and dark curves presents in **Figure S8**. The corresponding parameters of the devices are summarized in **Table 2**. As respected, the highest PCE of 7.5% with a short circuit current density (J_{sc}) of 15.80 mA cm^{-2}, an open circuit voltage (V_{oc}) of 0.730 V, a fill factor (FF) of 65.4% is achieved in the devices with ZnO/3%C60-PEG hybrids. However, the performance of the devices by employing ZnO/C60-PEG from blend approach as cathode buffer layer is worse than that of devices using ZnO@C60-PEG from growth approach as cathode buffer layer. The results should mainly result from the inferior morphology and charge transport of the blend films. In addition, the ZnO@C60-PEG from growth approach as cathode buffer layer can also favor a better interfacial content with the active layer than the blend approach, as depicted by different contact angles of the two types of hybrids (**Figure S9** and **Figure S10**), which can further contribute to the performance enhancement. Similar result is also found in the device with other type of active layer composed of poly(3-hexylthiophene) (P3HT): (6,6)-phenyl-C_{61} butyric acid methyl ester ($PC_{61}BM$) (**Figure S11, Figure S12** and **Table S4**). Furthermore, the CdS and CdS@C60-PEG were also applied to fabricate devices (**Figure S13** and **Table S5**), with the same tendency obtained. Moreover, due to the modification of C60-PEG to ZnO with less defects, inverted devices using two types of hybrids cathode buffer layer show a better stability than the devices with bare ZnO cathode buffer layer (**Figure S14**).

------- **Figure 8**-------

------**Table 2**------

3. Experimental

Materials

PEG (M_w=6000, Aladdin), poly(3-hexylthiophene) (P3HT, M_w = 60000-75000, Rieke Metals Inc), thieno[3,4-b]-thiophene/benzodithiophene (PTB7, 1-Materials), (6,6)-phenyl-C_{61} butyric acid methyl ester ($PC_{61}BM$ 99.5%; Nano-C),

triphenylphosphine (>99.0%; Aladdin), [6,6]-phenyl C_{71}-butyric acid methyl ester ($PC_{71}BM$, 99%, Nano-C), diethyl azodicarboxylate (>97.0%; Aladdin), zinc acetate dihydrate ($Zn(CH_3COO)_2 \cdot 2H_2O$, 99.9%, Aldrich), potassium hydroxide (KOH, 90%, AR, Aldrich), ethanolamine ($NH_3CH_2CH_2OH$, 99.5%, Aldrich) and 2-methoxyethanol ($CH_3OCH_2CH_2OH$, 99.8%, Aldrich) were used as received.

Synthesis of C60-PEG

The [6,6]-phenyl-C_{61}-butyric acid (PCBA) was obtained by the hydrolysis of PCBM according to the literature.[55] Then, PCBA (0.1 g, 0.112 mmol) and PEG (0.456 g, 0.076 mmol) were dissolved in the mixed solvent of 1,2-dichlorobenzene and methylbenzene (V:V=1:1) and the solution was sonicated for 1 h to dissolve PCBA completely. Triphenylphosphine (0.08 g, 0.290 mmol) and the diethyl azodicarboxylate (0.055 g, 0.290 mmol) was added dropwise to the solution. The reaction was held at room temperature for 2 days. After solvent removed, the products were purified by column chromatography with ethyl acetate and methyl alcohol.

Preparation of the ZnO@C60-PEG

The ZnO was synthesized following the process reported by Heeger et al.[17] The general procedure for the preparation of ZnO as follows: the ZnO precursor was prepared by dissolving 1 g $Zn(CH_3COO)_2 \cdot 2H_2O$ and 0.28 g $NH_3CH_2CH_2OH$ in 10 mL $CH_3OCH_2CH_2OH$ under vigorous stirring overnight for the hydrolysis reaction in air. Different ratio of C60-PEG was added to the ZnO precursor solution to obtain ZnO@C60-PEG precursor. Then, the ZnO@C60-PEG precursor was coat on the ITO substrate and annealed in air for 40 min at 150 °C to get the ZnO@C60-PEG.

Preparation of the ZnO/C60-PEG

ZnO was synthesized following the process reported by Beek et al.[37] The general procedure for the preparation of ZnO as follows: 1.23 g of $Zn(CH_3COO)_2 \cdot 2H_2O$ was dissolved in methanol (55 mL) at 60 °C under vigorous stirring. 25 mL of KOH solution (0.34 $mmol \cdot mL^{-1}$) was dropped into the $Zn(CH_3COO)_2 \cdot 2H_2O$ solution in 20

minutes under vigorous stirring. The reaction was held at 60 °C for additional 2 h to yield a homogeneous, clear, and transparent solution, and then left the solution alone to precipitate for another 2 h. Precipitate was separated by centrifugation and was washed twice with methanol. The ZnO nanoparticles disperse in $CH_3OCH_2CH_2OH$. Different ratio of C60-PEG was added into the ZnO solutions and sonicated for over half an hour.

Fabrication of inverted polymer solar cells

ITO-coated glass substrates (35 $\Omega \cdot cm^{-2}$) were cleaned with alcohol, detergent, deionized water and isopropyl, and dried by nitrogen flow followed by plasma treatment for 15 minutes. All cathode buffer layers were coated on the ITO-coated glass substrates. The blended solution P3HT:$PC_{61}BM$ (1:1 w/w, 1,2-dichlorobenzene, 60 °C) or PTB7:$PC_{71}BM$ (1:1.5 w/w, chlorobenzene/1,8-diiodooctane (97:3 v/v), 70 °C) was stirred in glovebox overnight, which was spin coated on top of the cathode buffer layer as active layer. Finally, anode buffer layer MoO_3 (7 nm) and anode Ag (90 nm) was deposited on the top of the active layer by thermal evaporation in a high vacuum (< 10^{-7} Torr). Current-voltage (*J-V*) characteristics were tested using Keithley 2400 Source Meter in the dark and under simulated AM 1.5 G (100 $mW \cdot cm^{-2}$) irradiation (Abet Solar Simulator Sun2000). Incident photon-to-current efficiency (IPCE) were measured under monochromatic illumination (Oriel Cornerstone 260 1/4 m monochromator equipped with Oriel 70613NS QTH lamp), and the calibration of the incident light was performed with a monocrystalline silicon diode.

Characterizations

Ultraviolet–visible (UV–vis) absorption spectra and was carried out by PerkinElmer Lambda 750 spectrophotometer. Hitachi F-7000 spectrofluorophotometer was applied for the measurements of photoluminescence (PL). The morphologies of the samples were measured by an atomic force microscope (AFM) (Digital Instrument Nanoscope 31) and a transmission electron microscopy (TEM; JEOL, JEM-2100F) which were recorded on holey carbon-coated copper grids. The crystallinity of the samples were

tested by the X-ray diffraction (XRD), using a Bruker D8 Focus X-ray diffractometer operating at 30 kV and 20 mA with a copper target (λ =1.54 Å) under a scanning rate of 1º/min. Ultraviolet photo-electron spectroscopy (UPS) and X-ray photoelectron spectroscopy (XPS) measurements were carried out by AXIS-ULTRA DLD spectrometer (Kratos Analytical Ltd.) using He (I) (21.2 eV) as monochromatic light source. The thicknesses of all the layers were measured by surface profilometry (Alpha-Step-IQ). Water contact angle measurements for all samples were taken on JC2000A contact angle instrument.

4. Conclusions

In conclusion, two types of novel fullerene derivative/ZnO hybrids were prepared by physical blend ZnO nanocrystals with C60-PEG and by *in situ* growth ZnO nanocrystals from C60-PEG. The C60-PEG produces an n-doping effect on ZnO and the oxygen-rich PEG side chain of C60-PEG passivate the defects of ZnO nanoparticles. At the same time, the addition of amphiphilic C60-PEG facilitates the compatibility of inorganic cathode buffer layer and organic active layer. In contrast to the bare ZnO, the two types of hybrids cathode buffer layer process decreased work function, less defects, higher electron mobility, which effectively reduces the recombination of carriers and enhances electron extraction. Consequently, the efficiency and stability of the inverted devices employing two types of ZnO hybrids as cathode buffer layers has been improved. Compared with the blend approach, growth approach of ZnO from C60-PEG shows better performance, due to its more favorable morphology, higher charge transport and improved contact with the active layer.

Supporting Information

The detailed experimental sections and the other characterization of devices are available. This information is available free of charge via the Internet at http://pubs.rsc.org.

Acknowledgements

This work was financially supported by the National Science Fund for Distinguished Young Scholars (51425304), National Natural Science Foundation of China (51273088, 51263016 and 51473075), and National Basic Research Program of China (973 Program 2014CB260409). Ting Hu and Lie Chen contributed equally to this work.

References

1. Y. Zhang, T. P. Basel, B. R. Gautam, X. Yang, D. J. Mascaro, F. Liu and Z. V. Vardeny, *Nat. Commun.*, 2012, **3**, 1043.
2. B. C. Thompson and J. M. J. Fréchet, *Angew Chem Int Edit*, 2008, **47**, 58-77.
3. F. C. Krebs, *Sol. Energy Mater. Sol. Cells*, 2009, **93**, 394-412.
4. B. Kan, Q. Zhang, M. Li, X. Wan, W. Ni, G. Long, Y. Wang, X. Yang, H. Feng and Y. Chen, *J. Am. Chem. Soc.*, 2014, **136**, 15529-15532.
5. W. Li, W. S. Roelofs, M. Turbiez, M. M. Wienk and R. A. Janssen, *Adv. Mater.*, 2014, **26**, 3304-3309.
6. Y. Liu, J. Zhao, Z. Li, C. Mu, W. Ma, H. Hu, K. Jiang, H. Lin, H. Ade and H. Yan, *Nat. Commun.*, 2014, **5**, 5293.
7. A. Sharenko, D. Gehrig, F. Laquai and T.-Q. Nguyen, *Chem. Mater.*, 2014, **26**, 4109-4118.
8. G. Li, V. Shrotriya, J. Huang, Y. Yao, T. Moriarty, K. Emery and Y. Yang, *Nat. Mater.*, 2005, **4**, 864-868.
9. J. Peet, M. L. Senatore, A. J. Heeger and G. C. Bazan, *Adv. Mater.*, 2009, **21**, 1521-1527.
10. C. E. Small, S. Chen, J. Subbiah, C. M. Amb, S.-W. Tsang, T.-H. Lai, J. R. Reynolds and F. So, *Nat. Photonics*, 2012, **6**, 115-120.
11. L. Dou, J. You, J. Yang, C.-C. Chen, Y. He, S. Murase, T. Moriarty, K. Emery, G. Li and Y. Yang, *Nat. Photonics*, 2012, **6**, 180-185.
12. Y. Liang, Z. Xu, J. Xia, S.-T. Tsai, Y. Wu, G. Li, C. Ray and L. Yu, *Adv. Mater.*, 2010, **22**, E135-E138.
13. H.-Y. Chen, J. Hou, S. Zhang, Y. Liang, G. Yang, Y. Yang, L. Yu, Y. Wu and G. Li, *Nat. Photonics*, 2009, **3**, 649-653.
14. C.-Y. Li, T.-C. Wen and T.-F. Guo, *J. Mater. Chem.*, 2008, **18**, 4478-4482.
15. K. Zilberberg, S. Trost, J. Meyer, A. Kahn, A. Behrendt, D. Lützenkirchen-Hecht, R. Frahm and T. Riedl, *Adv. Funct. Mater.*, 2011, **21**, 4776-4783.
16. D. Zhang, W. C. H. Choy, F. Xie, W. E. I. Sha, X. Li, B. Ding, K. Zhang, F. Huang and Y. Cao, *Adv. Funct. Mater.*, 2013, **23**, 4255-4261.
17. Y. Sun, J. H. Seo, C. J. Takacs, J. Seifter and A. J. Heeger, *Adv. Mater.*, 2011, **23**, 1679-1683.
18. A. W. Hains and T. J. Marks, *Appl. Phys. Lett.*, 2008, **92**.
19. A. W. Hains, J. Liu, A. B. F. Martinson, M. D. Irwin and T. J. Marks, *Adv. Funct. Mater.*, 2010, **20**, 595-606.
20. F. Huang, H. Wu, D. Wang, W. Yang and Y. Cao, *Chem. Mater.*, 2004, **16**, 708-716.
21. C. He, C. Zhong, H. Wu, R. Yang, W. Yang, F. Huang, G. C. Bazan and Y. Cao, *J. Mater. Chem.*, 2010, **20**, 2617-2622.
22. S.-H. Oh, S.-I. Na, J. Jo, B. Lim, D. Vak and D.-Y. Kim, *Adv. Funct. Mater.*, 2010, **20**, 1977-1983.

23. J. W. Jung, J. W. Jo and W. H. Jo, *Adv. Mater.*, 2011, **23**, 1782-1787.
24. Q. Wei, T. Nishizawa, K. Tajima and K. Hashimoto, *Adv. Mater.*, 2008, **20**, 2211-2216.
25. J. W. Jung, J. W. Jo and W. H. Jo, *Adv. Mater.*, 2011, **23**, 1782-1787.
26. D. Yang, L. Zhou, L. Chen, B. Zhao, J. Zhang and C. Li, *Chem. Commun.*, 2012, **48**, 8078-8080.
27. J. Liu, Y. Xue, Y. Gao, D. Yu, M. Durstock and L. Dai, *Adv. Mater.*, 2012, **24**, 2228-2233.
28. S.-S. Li, K.-H. Tu, C.-C. Lin, C.-W. Chen and M. Chhowalla, *ACS Nano*, 2010, **4**, 3169-3174.
29. Z. Ma, Z. Tang, E. Wang, M. R. Andersson, O. Inganäs and F. Zhang, *J. Phys. Chem. C*, 2012, **116**, 24462-24468.
30. Z. Liang, Q. Zhang, O. Wiranwetchayan, J. Xi, Z. Yang, K. Park, C. Li and G. Cao, *Adv. Funct. Mater.*, 2012, **22**, 2194-2201.
31. J. Liu, S. Shao, B. Meng, G. Fang, Z. Xie, L. Wang and X. Li, *Appl. Phys. Lett.*, 2012, **100**, 213906.
32. S. B. Jo, J. H. Lee, M. Sim, M. Kim, J. H. Park, Y. S. Choi, Y. Kim, S. G. Ihn and K. Cho, *Adv. Energy Mater.,* 2011, **1**, 690-698.
33. T. Hu, F. Li, K. Yuan and Y. Chen, *ACS Appl. Mater. Interfaces*, 2013, **5**, 5763-5770.
34. S. Shao, K. Zheng, T. Pullerits and F. Zhang, *ACS Appl. Mater. Interfaces*, 2013, **5**, 380-385.
35. C.-H. Hsieh, Y.-J. Cheng, P.-J. Li, C.-H. Chen, M. Dubosc, R.-M. Liang and C.-S. Hsu, *J. Am. Chem. Soc.*, 2010, **132**, 4887-4893.
36. B. Neises and W. Steglich, *Angew. Chem. Int. Ed.*, 1978, **17**, 522-524.
37. W. J. Beek, M. M. Wienk, M. Kemerink, X. Yang and R. A. Janssen, *J. Phys. Chem. B*, 2005, **109**, 9505-9516.
38. L. E. Greene, M. Law, J. Goldberger, F. Kim, J. C. Johnson, Y. Zhang, R. J. Saykally and P. Yang, *Angew. Chem. Int. Ed.*, 2003, **42**, 3031-3034.
39. H. C. Leventis, S. P. King, A. Sudlow, M. S. Hill, K. C. Molloy and S. A. Haque, *Nano Lett.*, 2010, **10**, 1253-1258.
40. Q. Wan, K. Yu, T. H. Wang and C. L. Lin, *Appl. Phys. Lett.*, 2003, **83**, 2253-2255.
41. D. Gao, J. Zhang, G. Yang, J. Zhang, Z. Shi, J. Qi, Z. Zhang and D. Xue, *J. Phys. Chem. C*, 2010, **114**, 13477-13481.
42. S. H. Liao, H. J. Jhuo, Y. S. Cheng and S. A. Chen, *Adv. Mater.*, 2013, **25**, 4766-4771.
43. X. W. M. Chen , Y. H. Yu , Z. L. Pei , X. D. Bai , C. Sun , R. F. Huang , and L. S., *Appl. Surf. Sci.*, 2000, 158, 134-140..
44. A. van Dijken, E. A. Meulenkamp, D. Vanmaekelbergh and A. Meijerink, *J. Phys. Chem. B*, 2000, **104**, 4355-4360.
45. A. van Dijken, E. A. Meulenkamp, D. Vanmaekelbergh and A. Meijerink, *J. Phys. Chem. B*, 2000, **104**, 1715-1723.
46. H. Zeng, G. Duan, Y. Li, S. Yang, X. Xu and W. Cai, *Adv. Funct. Mater.*, 2010,

20, 561-572.
47. X. Sui, C. Shao and Y. Liu, *Polymer*, 2007, **48**, 1459-1463.
48. J. H. Seo, R. Yang, J. Z. Brzezinski, B. Walker, G. C. Bazan and T.-Q. Nguyen, *Adv. Mater.*, 2009, **21**, 1006-1011.
49. S. Braun, W. R. Salaneck and M. Fahlman, *Adv Mater*, 2009, **21**, 1450-1472.
50. K. Woo, Y. Kim and J. Moon, *Energy Environ. Sci.*, 2012, **5**, 5340-5345.
51. T. B. Yang, M. Wang, C. H. Duan, X. W. Hu, L. Huang, J. B. Peng, F. Huang and X. Gong, *Energy Environ. Sci.*, 2012, **5**, 8208-8214.
52. J. S. Park, J. M. Lee, S. K. Hwang, S. H. Lee, H. J. Lee, B. R. Lee, H. I. Park, J. S. Kim, S. Yoo, M. H. Song and S. O. Kim, *J. Mater. Chem.*, 2012, **22**, 12695-12700.
53. H.-Y. Park, D. Lim, K.-D. Kim and S.-Y. Jang, *J. Mater. Chem. A*, 2013, **1**, 6327.
54. X. Gong, M. Tong, F. G. Brunetti, J. Seo, Y. Sun, D. Moses, F. Wudl and A. J. Heeger, *Adv. Mater.*, 2011, **23**, 2272-2277.
55. J. C. Hummelen, B. W. Knight, F. LePeq, F. Wudl, J. Yao and C. L. Wilkins, *J. Org. Chem.*, 1995, **60**, 532-538.

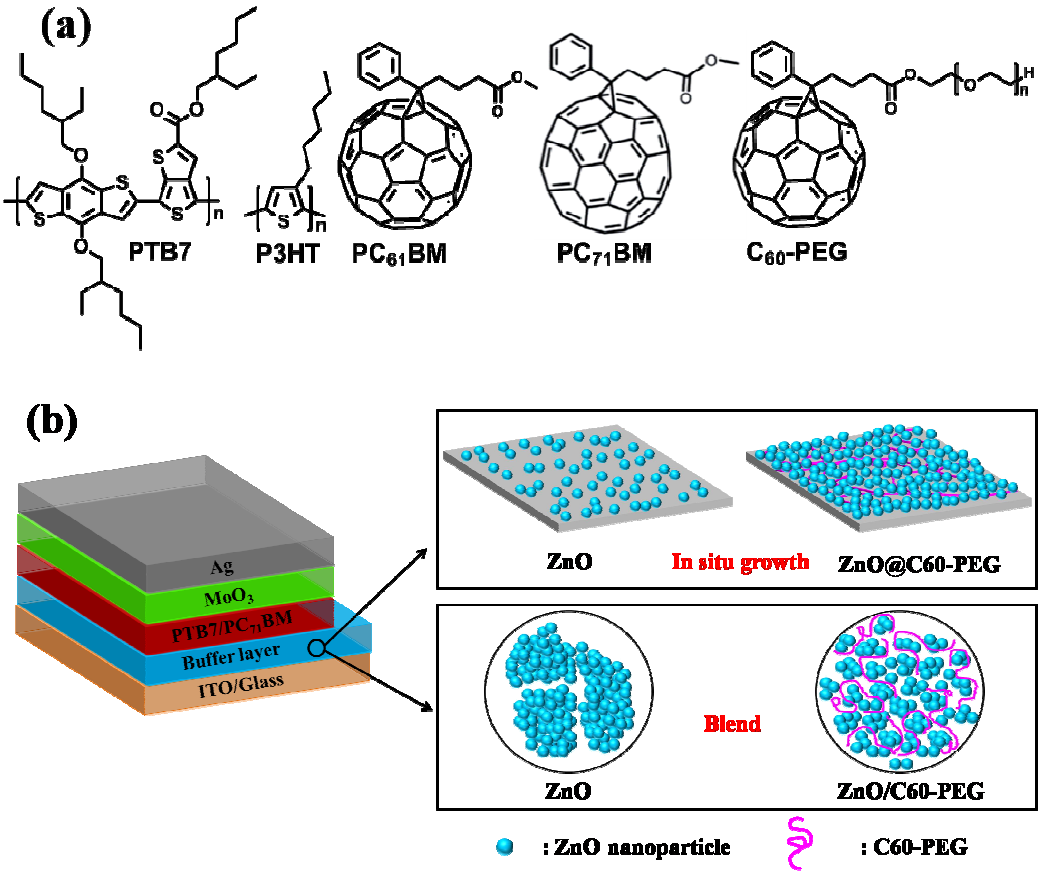

Figure 1. (a) Chemical structures of the materials used for device fabrication. (b) The structure of device and the schematic diagram of two types fullerene derivative/ZnO hybrids.

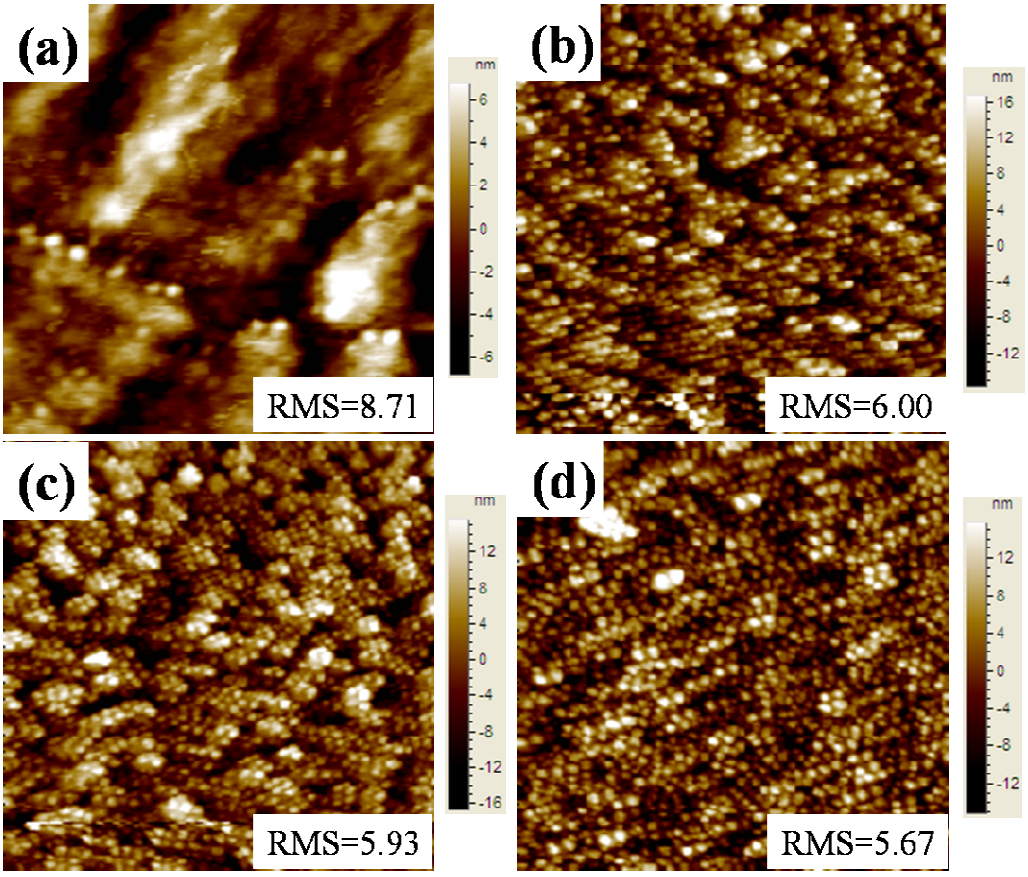

Figure 2. AFM height images (5μm×5μm) of (a) ZnO, (b) ZnO/1%C60-PEG, (c) ZnO/3%C60-PEG and (d) ZnO/5%C60-PEG. The inset of every image is the roughness value of root-mean-square (RMS).

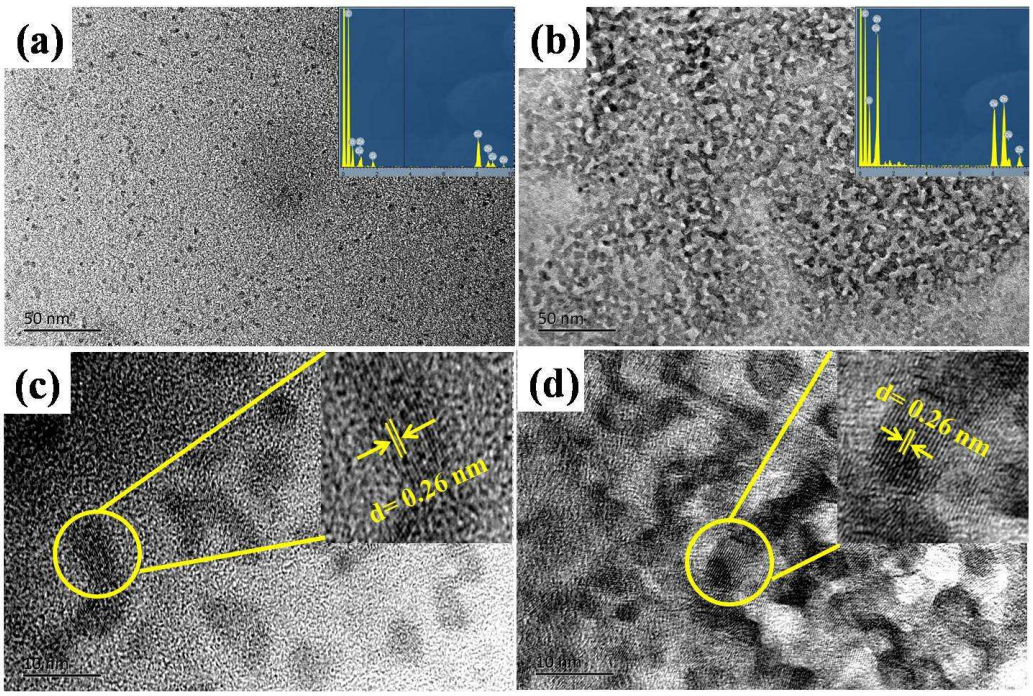

Figure 3. TEM images of (a) ZnO and (b) ZnO@1%C60-PEG. The inset of (a) and (b) show the EDX spectrum, which confirms the presence of ZnO. The corresponding HRTEM images are shown in (c) ZnO and (d) ZnO@1%C60-PEG. The inset of (c) and (d) show the lattice fringes image of a ZnO nanocrystals.

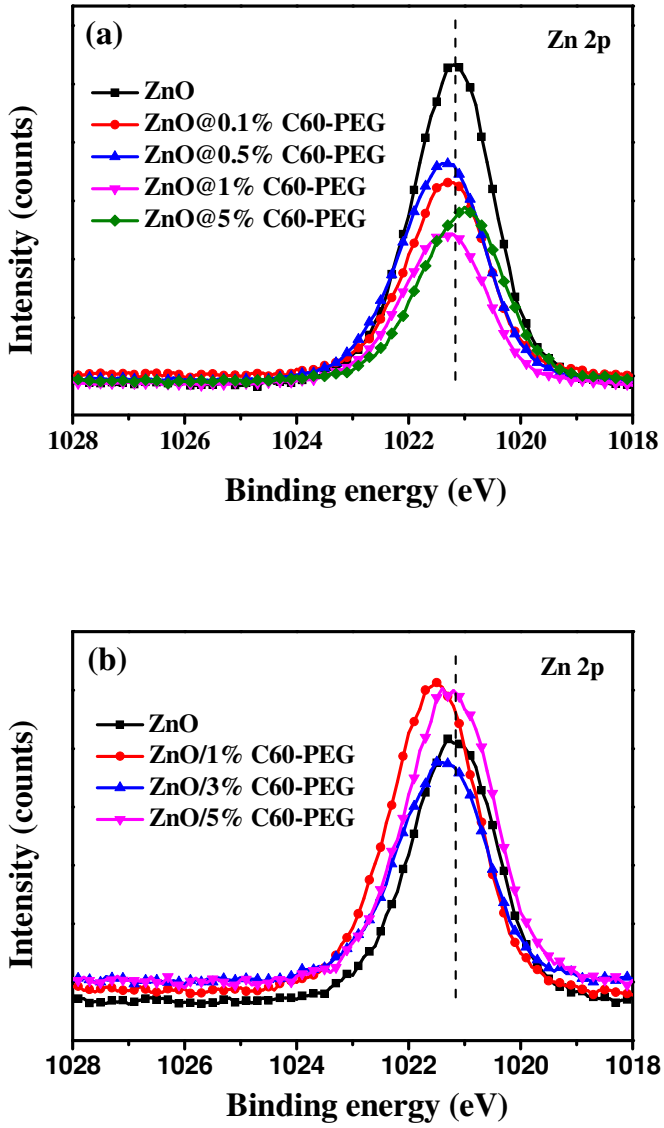

Figure 4. (a) Zn 2p XPS spectra of ZnO, ZnO@0.1%C60-PEG, ZnO@0.5%C60-PEG, ZnO@1%C60-PEG and ZnO@5%C60-PEG. (b) Zn 2p XPS spectra of ZnO, ZnO/1%C60-PEG, ZnO/3%C60-PEG and ZnO/5%C60-PEG.

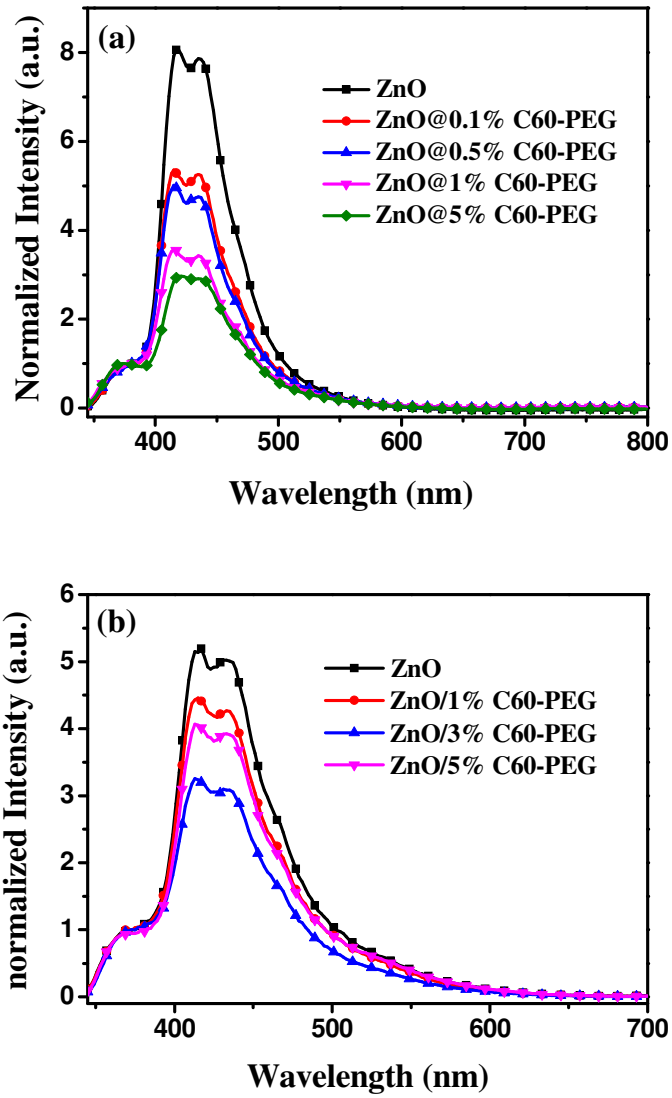

Figure 5. (a) Normalized photoluminescence spectra of ZnO, ZnO@0.1%C60-PEG, ZnO@0.5%C60-PEG, ZnO@1%C60-PEG and ZnO@5%C60-PEG under photoexcitation at 325 nm. (b) Normalized photoluminescence spectra of ZnO, ZnO/1%C60-PEG, ZnO/3%C60-PEG and ZnO/5%C60-PEG under photoexcitation at 325 nm.

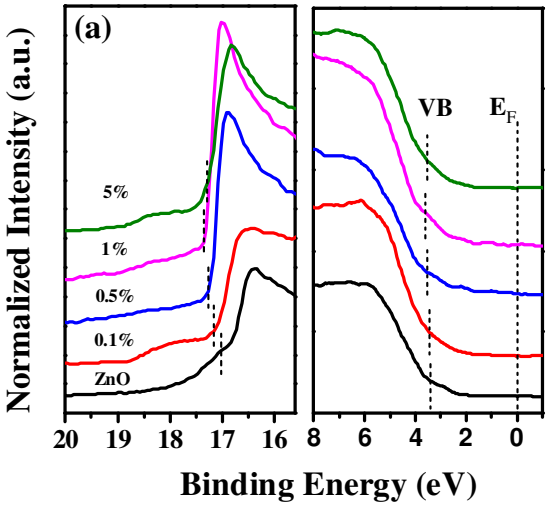

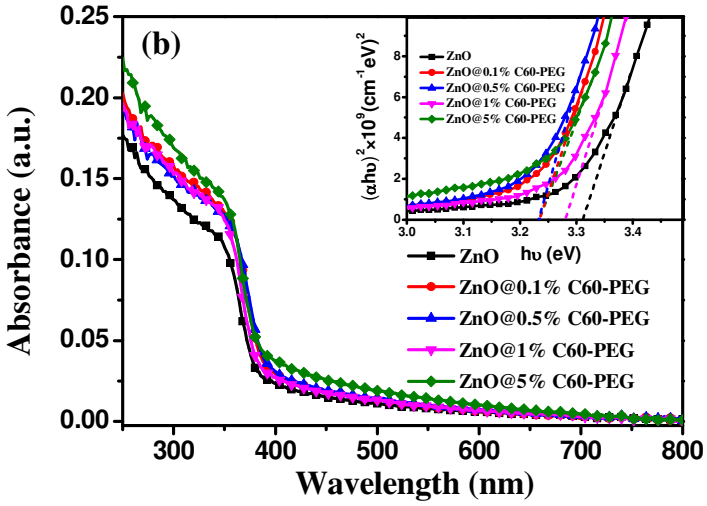

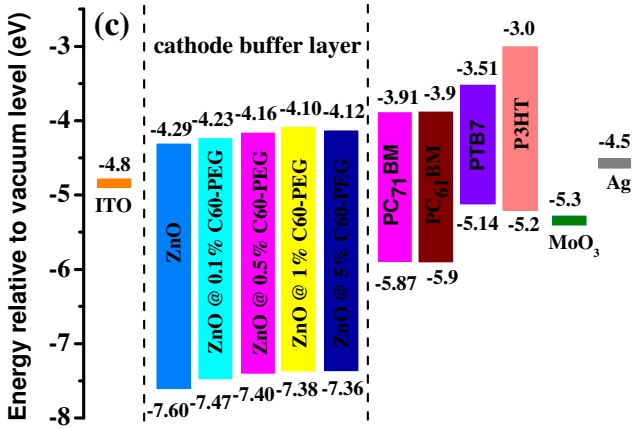

Figure 6. (a) UPS spectra and (b) UV–vis absorbance spectra (the inset is plots of $(\alpha h\nu)^2$ versus energy) of ZnO, ZnO@0.1%C60-PEG, ZnO@0.5%C60-PEG, ZnO@1%C60-PEG and ZnO@5%C60-PEG; (c) the corresponding energy level diagram of the components of the devices.

Table 1. Energy levels of ZnO, ZnO@0.1%C60-PEG, ZnO@0.5%C60-PEG, ZnO@1%C60-PEG and ZnO@5%C60-PEG.

Buffer layer	Eg (UV-Vis)	HOMO (UPS)	LUMO (Eg)
ZnO	3.31	7.60	4.29
ZnO@0.1% C60-PEG	3.24	7.47	4.23
ZnO@0.5% C60-PEG	3.24	7.40	4.16
ZnO@1% C60-PEG	3.28	7.38	4.10
ZnO@5% C60-PEG	3.24	7.36	4.12

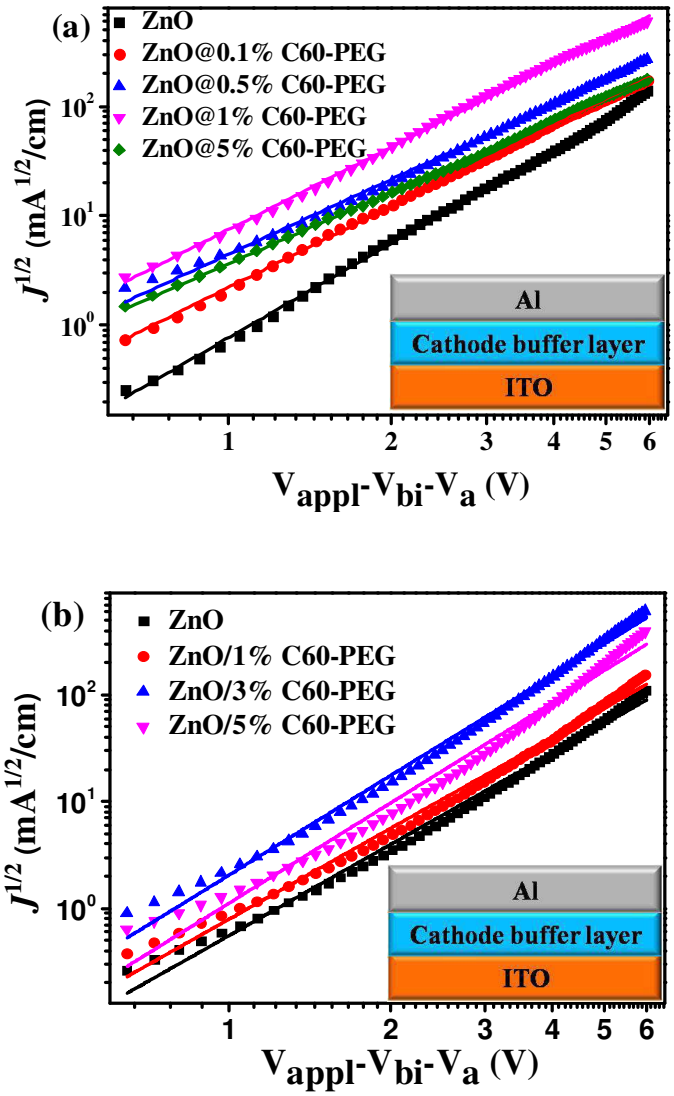

Figure 7. Log *J vs.* log *V* plots for Mott–Gurney SCLC fitting of the electron-only devices for (a) ZnO, ZnO@0.1%C60-PEG, ZnO@0.5%C60-PEG, ZnO@1%C60-PEG and ZnO@5%C60-PEG, (b) ZnO, ZnO/1%C60-PEG, ZnO/3%C60-PEG and ZnO/5%C60-PEG with a structure of ITO/cathode buffer layer/Al. The inset shows the configuration of the electron-only device.

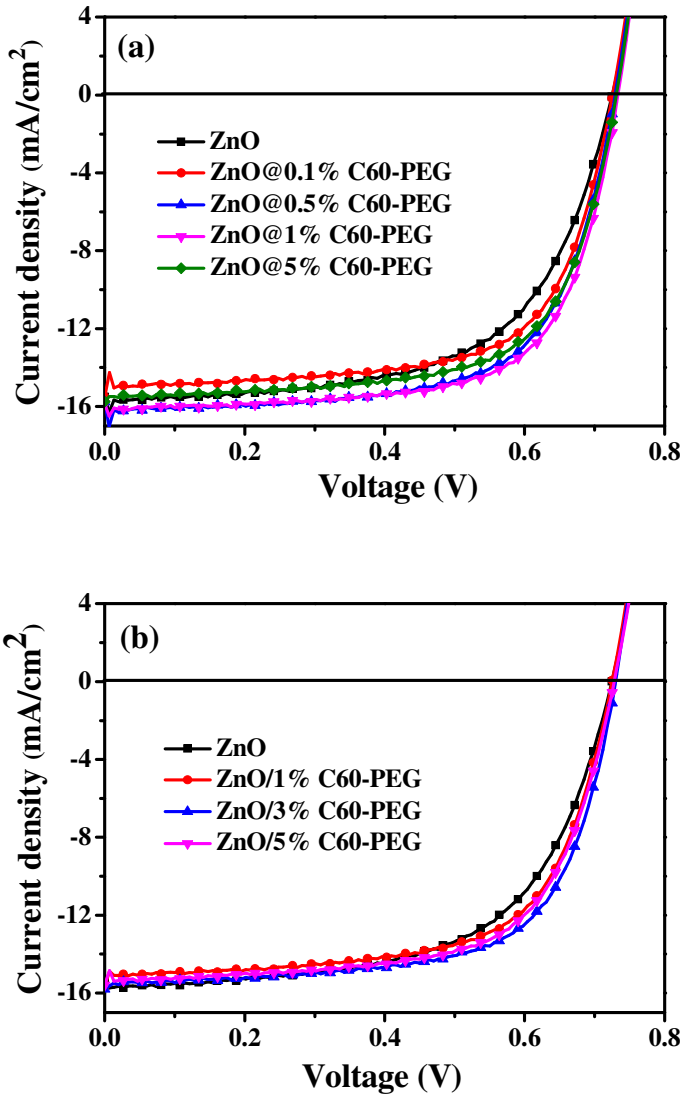

Figure 8. Illuminated *J-V* characteristics of the devices ITO/cathode buffer layer/PTB7:$PC_{71}BM$/MoO_3/Ag by using (a) ZnO, ZnO@0.1%C60-PEG, ZnO@0.5%C60-PEG, ZnO@1%C60-PEG and ZnO@5%C60-PEG, (b) ZnO, ZnO/1%C60-PEG, ZnO/3%C60-PEG and ZnO/5%C60-PEG as cathode buffer layer.

Table 2. Photovoltaic parameters of the devices with ITO/cathode buffer layer/PTB7:$PC_{71}BM$/MoO_3/Ag structure. [a]All data of devices had been tested from more than five substrates (20 chips) to ensure reproducibility. [b]The ZnO was synthesized following the process reported by Heeger *et al*. [c]The ZnO was synthesized following the process reported by Beek *et al*.

Device[a]	J_{sc} [mA cm^{-2}]	V_{oc} [V]	FF [%]	PCE [%]
ZnO[b]	15.51±0.10	0.724±0.003	61.4±1.2	6.9±0.1
ZnO@0.1%C60-PEG	15.52±0.14	0.725±0.002	64.5±1.1	7.3±0.2
ZnO@0.5%C60-PEG	15.77±0.11	0.729±0.002	68.1±1.0	7.8±0.1
ZnO@1%C60-PEG	**15.86±0.12**	**0.733±0.004**	**69.1±1.2**	**8.0±0.1**
ZnO@5%C60-PEG	15.76±0.10	0.731±0.003	65.6±1.2	7.6±0.1
ZnO[c]	15.44±0.12	0.724±0.003	61.2±1.1	6.8±0.1
ZnO/1%C60-PEG	15.67±0.14	0.725±0.002	63.1±1.4	7.2±0.2
ZnO/3%C60-PEG	**15.80±0.13**	**0.730±0.004**	**65.4±1.5**	**7.5±02**
ZnO/5%C60-PEG	15.59±0.12	0.728±0.002	64.7±1.3	7.3±0.1

Highlights

Amphiphilic Fullerenes/ZnO Hybrids as Cathode Buffer Layer to Improve Charge Selectivity of Inverted Polymer Solar Cells

Ting Hu, Lie Chen, Kai Yuan, Yiwang Chen*

The novel fullerene derivative/ZnO hybrids are prepared as cathode buffer layers for improving the performance of inverted polymer solar cells.

Graphical abstract